

Probing the high-density behavior of symmetry energy with gravitational waves

F. J. Fattoyev¹, W. G. Newton¹ and Bao-An Li¹

Department of Physics and Astronomy, Texas A&M University-Commerce, Commerce, TX 75429, USA

Received: date / Revised version: date

Abstract. Gravitational wave (GW) astronomy opens up an entirely new window on the Universe to probe the equations of state (EOS) of neutron-rich matter. With the advent of next generation GW detectors, measuring the gravitational radiation from coalescing binary neutron star systems, mountains on rotating neutron stars, and stellar oscillation modes may become possible in the near future. Using a set of model EOSs satisfying the latest constraints from terrestrial nuclear experiments, state of the art nuclear many-body calculations of the pure neutron matter EOS, and astrophysical observations consistently, we study various GW signatures of the high-density behavior of the nuclear symmetry energy, which is considered among the most uncertain properties of dense neutron-rich nucleonic matter. In particular, we find the tidal polarizability of neutron stars, potentially measurable in binary systems just prior to merger, is more sensitive to the high density component of the nuclear symmetry energy than the symmetry energy at nuclear saturation density. We also find that the upper limit on the GW strain amplitude from elliptically deformed stars is very sensitive to the density dependence of the symmetry energy. This suggests that future developments in modeling of the neutron star crust, and direct gravitational wave signals from accreting binaries will provide a wealth of information on the EOS of neutron-rich matter. We also review the sensitivity of the r -mode instability window to the density dependence of the symmetry energy. Whereas models with larger values of the density slope of the symmetry energy at saturation seem to be disfavored by the current observational data, within a simple r -mode model, we point out that a subsequent softer behavior of the symmetry energy at high densities (hinted at by recent observational interpretations) could rule them in.

PACS. 04.30.-w Gravitational waves – 04.40.Dg Relativistic stars: structure, stability, and oscillations – 21.65.Ef Symmetry energy – 26.60.Kp Equations of state of neutron-star matter – 97.60.Jd Neutron stars

1 Introduction

Understanding the nature of the neutron-rich nucleonic matter is one of the fundamental quests of both nuclear physics and astrophysics [1]. To fulfill this goal, many experiments and observations are being carried out or proposed using a wide variety of advanced new facilities, such as the Facility for Rare Isotope Beams (FRIB), telescopes operating at a variety of wavelengths, and more sensitive GW detectors (such as Advanced LIGO-Virgo). The EOS of neutron-rich matter is a vital ingredient in the interpretation of the results of these experiments and observations. Within the parabolic approximation the EOS can be written in terms of the binding energy per nucleon $E(\rho, \alpha)$ as

$$E(\rho, \alpha) = E(\rho, 0) + S(\rho)\alpha^2, \quad (1)$$

where $\alpha = (\rho_n - \rho_p)/\rho$ is the isospin asymmetry, $E(\rho, 0)$ is the binding energy per nucleon in symmetric nuclear matter (SNM), and $S(\rho)$ is the symmetry energy which represents the energy cost per nucleon of changing all the

protons in SNM into neutrons. Around the saturation density ρ_0 , one can make further expansions:

$$E(\rho, 0) = B + \frac{1}{2}K_0\chi^2 + \mathcal{O}(\chi^3), \quad (2)$$

$$S(\rho) = J + L\chi + \frac{1}{2}K_{\text{sym}}\chi^2 + \mathcal{O}(\chi^3), \quad (3)$$

where $\chi \equiv (\rho - \rho_0)/3\rho_0$, B and K_0 are the binding energy per nucleon and the nuclear incompressibility at saturation density, ρ_0 , while J , L , and K_{sym} are the corresponding magnitude, slope, and curvature of the symmetry energy at saturation density. Whereas significant progress has been achieved in constraining the EOS of SNM around $\rho \approx \rho_0$, its density dependence remains still rather uncertain for nuclear matter at high densities and with large isospin asymmetries. Observationally, the best constraint on the high-density component of the EOS comes from the largest observed masses of neutron stars that have been recently reported by Demorest *et al.* [2] and Antoniadis *et al.* [3]. Combining observational results with terrestrial experimental studies of the collective flow and kaon pro-

duction in relativistic heavy-ion collisions [4] the EOS of SNM has been limited to a relatively small range up to about $4.5 \rho_0$. The main source of uncertainties in the EOS of neutron-rich matter therefore mostly comes from the poorly known density dependence of the nuclear symmetry energy $S(\rho)$, which is a vital ingredient in describing the structure of rare isotopes and their reaction mechanisms. Moreover, it determines uniquely the proton fraction and therefore the condition for the onset of the direct Urca process in neutron stars, affects significantly structural properties such as the radii, moments of inertia and the crust thickness, as well as the frequencies and damping times of various oscillation modes of neutron stars (see Refs. [5, 6, 7] for review).

Intensive efforts devoted to constraining $S(\rho)$ using various approaches have recently led to a close convergence [7, 8, 9, 10, 11, 12, 13] around $J \approx 30$ MeV and its density slope of $L \approx 60$ MeV, although the associated error-bars from different approaches may vary broadly. However, the possibility that J and L can be significantly different from these currently inferred values cannot be conclusively ruled out (See Ref. [14] for a detailed discussion). On the other hand, the high-density behavior of $S(\rho)$ remains quite uncertain despite its importance to understanding what happens in the core of neutron stars [15, 16, 17, 18, 19] and in reactions with high energy radioactive beams [20]. The predictions for the high-density behavior of the symmetry energy from all varieties of nuclear models diverge dramatically [21, 22, 23]. Some models predict very stiff symmetry energies that monotonically increase with density [23, 24, 25, 26, 27, 28], while others predict relatively soft ones, or an $S(\rho)$ that first increases with density, then saturates and starts decreasing with increasing density [21, 29, 30, 31, 32, 33, 34, 35, 36, 37, 38, 39, 40, 41, 42, 43]. These uncertainties can be associated with our poor knowledge about the isospin dependence of the strong interaction in the dense neutron-rich medium, particularly the spin-isospin dependence of many-body forces, the short-range behavior of the nuclear tensor force and the isospin dependence of nucleon-nucleon correlations in the dense medium, see, e.g. Refs. [44, 45]. The experimental progress in constraining the high density $S(\rho)$ is also limited partially due to the lack of sensitive probes. Whereas several observables have been proposed [20] and some indications of the high-density $S(\rho)$ have been reported recently [46, 47], conclusions based on terrestrial nuclear experiments remain highly controversial [48]. Interestingly, it was recently proposed that the late time neutrino signal from a core collapse supernova [49] and the tidal polarizability [50] of canonical neutron stars in coalescing binaries are very sensitive probes of the high-density behavior of nuclear symmetry energy, suggesting that astrophysical measurements might bolster experimental results in this area.

In this survey we focus on the sensitivity of various gravitational wave signals from neutron stars to the high-density component of the nuclear symmetry energy. Gravitational waves are oscillations of space-time and are one of the fundamental predictions of the theory of general relativity.

Although they have not been directly detected yet, there are strong indirect evidence that gravitational radiation exists. The highly accurate matching of the observed decrease in the orbital period of the celebrated Hulse-Taylor [51] and PSR J0737-3039 binary systems [69, 70] with the predicted value due to the energy loss through gravitational radiation serves as the most precise indirect evidence of the existence of gravitational waves. Because of their extremely weak interaction with matter, gravitational waves carry much cleaner information of their source as opposed to their electromagnetic counterparts, and therefore open an entirely new window to probe physics that is hidden to current electromagnetic observations. Of course, this property also makes their detection one of the most difficult experimental problems faced in physics today.

The manuscript has been organized as follows. In Section 2 we describe the formalism of constraining the EOS of SNM, and discuss the emergence of uncertainties in the high-density component of the EOS of neutron-rich matter due to the density dependence of symmetry energy. In Section 3 we present results for the selected gravitational wave signatures from neutron stars that are investigated consistently with the same set of EOSs discussed in Section 2. In particular, we study the sensitivity of gravitational waves generated by ellipticities in the neutron star shape generated by tidal polarization and mountains of accreted material, and by r -mode oscillations, to the high-density component of the nuclear symmetry energy. Finally, our concluding remarks are summarized in Section 4.

2 Constraining EOS of neutron-rich nuclear matter

We will concentrate on two models of the nuclear energy density functionals (EDF): the relativistic mean-field (RMF) model and the Skyrme Hartree-Fock (SHF) approach [13, 50]. For detailed discussion on these EDFs see the contributions to this volume by Nazarewicz *et al.* and by Piekarewicz. All of the EOSs used in this work are adjusted to satisfy the following four conditions within their respective known uncertain ranges:

- 1) Reproducing the EOS of pure neutron matter (PNM) at sub-saturation densities predicted by the latest state of the art microscopic nuclear many-body calculations [30, 52, 53, 54, 55, 56, 57];
- 2) Predicting correctly saturation properties of symmetric nuclear matter, *i.e.*, nucleon binding energy $B = -16 \pm 1$ MeV, incompressibility of nuclear matter $K_0 = 230 \pm 20$ MeV [58, 59], and the nucleon (Dirac) effective mass $M_{D,0}^* = 0.61 \pm 0.03 M$ [60] at saturation density $\rho_0 = 0.155 \pm 0.01 \text{ fm}^{-3}$;
- 3) Predicting a fiducial value of the symmetry energy $\tilde{J} = 26 \pm 0.5$ MeV at a subsaturation density of $2\rho_0/3$. Notice that theoretical microscopic PNM calculations also put tight constraints on both the symmetry energy and its density slope at saturation density: $J =$

31 ± 2 MeV and the density slope of the symmetry energy $L = 50 \pm 10$ MeV (See Ref. [13] and references therein). Also note that this range is a model dependent prediction coming from the theoretical constraints of PNM, that has no experimental analog;

- 4) Passing through the terrestrial constraints on the EOS of SNM between $2\rho_0$ and $4.5\rho_0$ [4] and predicting a maximum observed mass of neutron stars of about $2M_\odot$ assuming they are made of the nucleons (neutrons and protons) and light leptons (electrons and muons) only and without considering other degrees of freedom or invoking any exotic mechanism [2,3].

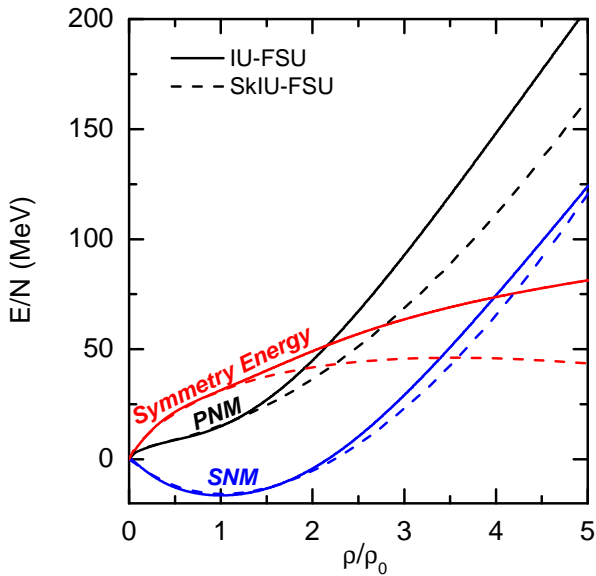


Fig. 1. (Color online) The EOS of SNM and PNM as well as the symmetry energy as a function of density obtained within the IU-FSU RMF model and the SHF approach using the SkIU-FSU parameter set. Taken from Ref. [50].

As an example, two EOSs were obtained using the IU-FSU parametrization of the RMF model [61] and its SHF counterpart dubbed as the SkIU-FSU parameter set [13], which are shown in Fig. 1. By design, they both have the same EOS for SNM and PNM around and below ρ_0 . Thus, at sub-saturation densities the values of $S(\rho)$ which is approximately the difference between the EOSs for PNM and SNM are almost identical for the two models. However, the values of $S(\rho)$ are significantly different above about $1.5\rho_0$ with the IU-FSU leading to a much stiffer $S(\rho)$ at high densities. As discussed in Ref. [13] this is due to the characteristic differences in the functional forms of the symmetry energy and is a generic feature of RMF and SHF models:

$$S_{\text{RMF}}(\rho) = A(\rho)\rho^{2/3} + B(\rho)\rho, \quad (4)$$

$$S_{\text{SHF}}(\rho) = a\rho^{2/3} - b\rho - c\rho^{5/3} - d\rho^{\sigma+1}, \quad (5)$$

where $A(\rho)$ and $B(\rho)$ are positive-valued functions of density, a , b , c , d and σ are some constant functions that may depend on Skyrme parameters only (for example, σ is just

a Skyrme parameter). The symmetry energy in the RMF model is therefore always positive, while certain terms of the symmetry energy in the SHF model can become negative at higher densities. More quantitatively, the $S(\rho)$ with IU-FSU is 40 to 60% higher in the density range of $3\rho_0$ to $4\rho_0$ expected to be attained in the core of canonical neutron stars.

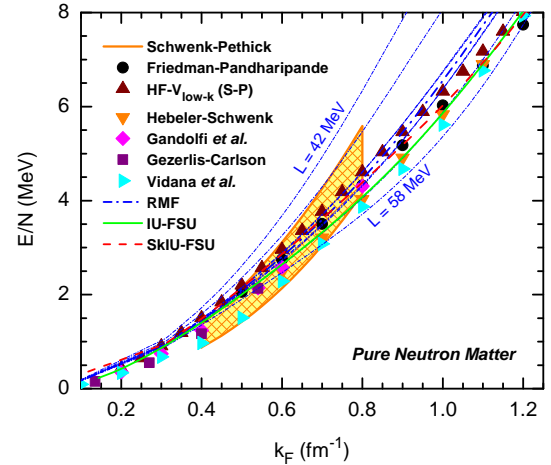


Fig. 2. (Color online) Energy per nucleon as a function of the Fermi momentum for PNM for selected models described in the text (Taken from Ref. [50]).

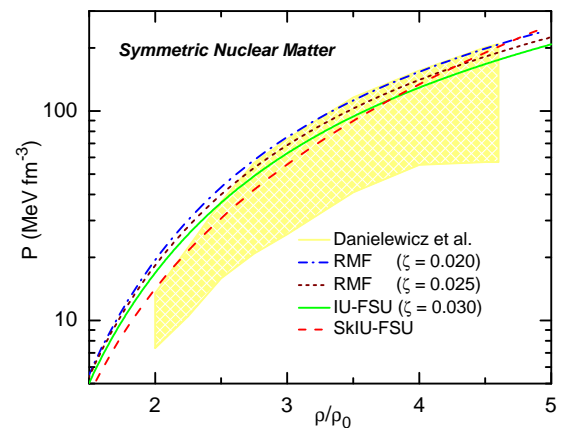


Fig. 3. (Color online) The pressure of SNM as a function of baryon density. Here ρ_0 is the nuclear matter saturation density and the shaded area represents the EOS extracted from the analysis of [4]. The figure is taken from Ref. [50].

To test the sensitivity of the various gravitational wave observables to variations of properties of neutron-rich nuclear matter around ρ_0 within the constraints listed above,

we also build seventeen different RMF parameterizations by systematically varying the values of K_0 , M_0^* , L , and the ζ parameter of the RMF model that controls the quartic omega-meson self interactions [62] and subsequently the high-density component of the EOS of SNM (See Table 1 for their predictions). Besides the constraints listed above, all parameterizations can correctly reproduce the experimental values for the binding energy and charge radius of ^{208}Pb and the ground state properties of other doubly magic nuclei within 2% accuracy [63]. As a reference for comparisons, we select $K_0 = 230$ MeV, $M_0^* = 0.61 M$, $L = 50$ MeV, and $\zeta = 0.025$ which we refer to as our baseline model. This model predicts $\rho_0 = 0.1524 \text{ fm}^{-3}$, $B = -16.33$ MeV and $J = 31.64$ MeV. The representative model EOSs for PNM at sub-saturation densities and those for SNM at supra-saturation densities are then compared with their constraints in Fig. 2 and Fig. 3, respectively. It is seen that the SkIU-FSU and all the RMF models with $42 < L < 58$ MeV can satisfy the constraint from the PNM EOS. Also, they all simultaneously satisfy the high density SNM EOS constraint with $0.02 < \zeta < 0.03$. Moreover, they all give a maximum mass for neutron stars in a range between $1.94M_\odot$ and $2.07M_\odot$ [61], the upper end of which is consistent with existing precise observational measurements [2,3]. While the determination of neutron-star radii from observations is both challenging and hindered by uncertainties in models of the stellar atmosphere amongst other things, significant advances in X-ray astronomy have allowed the simultaneous determination of masses and radii from a systematic study of several X-ray bursters. By assuming that all neutron stars have the same radius Guillot *et. al* [64] have recently analyzed the thermal spectra of 5 quiescent low-mass X-ray binaries in globular clusters to find that neutron star have radii of $R = 9.1^{+1.3}_{-1.5}$ km at a 90% confidence level. A subsequent re-analysis using Bayesian approach by Lattimer and Steiner [65] suggests that different interpretations of the data is strongly favored and they find much larger neutron star radii of $R = 12.1^{+0.7}_{-0.7}$ km for a 1.4 solar mass neutron star; neither range can currently be conclusively ruled out. The models discussed in our text predict canonical neutron star radii between 12.33 km and 13.22 km in the range of currently observed values [64,65,66,67,68].

3 Gravitational waves signals

3.1 Tidal Love number and polarizability

Coalescing binary neutron stars are among the most promising sources of laser-interferometric gravitational waves. One of the most important features of binary mergers is the tidal deformation neutron stars experience as they approach each other prior to merger. The strength of the tidal deformation can give us invaluable information about the neutron-star matter EOS [71,72,73,74,75,76,77,78,79,80,81,82]. At the early stage of an inspiral tidal effects may be effectively described through the tidal polarizability parameter λ [71,76,74,75] defined via

$$Q_{ij} = -\lambda \mathcal{E}_{ij}, \quad (6)$$

where Q_{ij} is the induced quadrupole moment of a star in binary due to the static external tidal field of the companion star \mathcal{E}_{ij} . The tidal polarizability can be expressed in terms of the dimensionless quadrupolar tidal Love number k_2 :

$$\lambda = \frac{2}{3} R^5 k_2, \quad (7)$$

where R is the radius of a neutron star in isolation, *i.e.* long before the merger. The tidal Love number k_2 depends on the stellar structure and can be calculated using the following expression [72,77]:

$$k_2 = \frac{1}{20} \left(\frac{R_s}{R}\right)^5 \left(1 - \frac{R_s}{R}\right)^2 \left[2 - y_R + (y_R - 1) \frac{R_s}{R}\right] \times \\ \times \left\{ \frac{R_s}{R} \left(6 - 3y_R + \frac{3R_s}{2R} (5y_R - 8) + \frac{1}{4} \left(\frac{R_s}{R}\right)^2 \left[26 - \right. \right. \right. \\ \left. \left. \left. - 22y_R + \left(\frac{R_s}{R}\right) (3y_R - 2) + \left(\frac{R_s}{R}\right)^2 (1 + y_R)\right]\right) \right\} + \\ + 3 \left(1 - \frac{R_s}{R}\right)^2 \left[2 - y_R + (y_R - 1) \frac{R_s}{R}\right] \times \\ \times \log \left(1 - \frac{R_s}{R}\right) \Big\}^{-1}, \quad (8)$$

where $R_s \equiv 2M$ is the Schwarzschild radius of the star, and $y_R \equiv y(R)$ can be calculated by solving the following first-order differential equation:

$$r \frac{dy(r)}{dr} + y(r)^2 + y(r)F(r) + r^2 Q(r) = 0, \quad (9)$$

with

$$F(r) = \frac{r - 4\pi r^3 (\mathcal{E}(r) - P(r))}{r - 2M(r)}, \quad (10)$$

$$Q(r) = \frac{4\pi r \left(5\mathcal{E}(r) + 9P(r) + \frac{\mathcal{E}(r)+P(r)}{\partial P(r)/\partial \mathcal{E}(r)} - \frac{6}{4\pi r^2}\right)}{r - 2M(r)} - \\ - 4 \left[\frac{M(r) + 4\pi r^3 P(r)}{r^2 (1 - 2M(r)/r)} \right]^2. \quad (11)$$

The Eq. (9) must be integrated together with the Tolman-Oppenheimer-Volkoff (TOV) equation. That is,

$$\frac{dP(r)}{dr} = - \frac{(\mathcal{E}(r) + P(r)) (M(r) + 4\pi r^3 P(r))}{r^2 (1 - 2M(r)/r)}, \quad (12)$$

$$\frac{dM(r)}{dr} = 4\pi r^2 \mathcal{E}(r). \quad (13)$$

Given the boundary conditions in terms of $y(0) = 2$, $P(0) = P_c$ and $M(0) = 0$, the tidal Love number can be obtained once an EOS is supplied. Previous studies have used both polytropic EOSs and several popular nuclear EOSs available in the literature [71,72,73,74,75,76,77,78,79,80,81,82]. While other particles may be present, it is

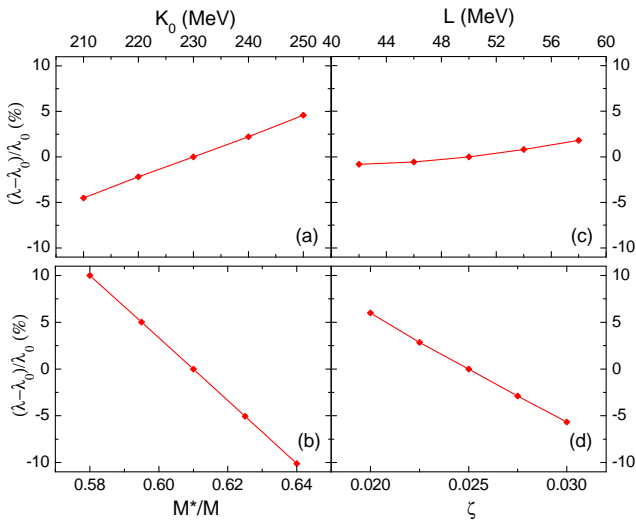


Fig. 4. (Color online) Percentage changes in the tidal polarizability of a canonical 1.4 solar mass neutron star by individually varying properties of nuclear matter K_0 (a), M^* (b), L (c), and the ζ parameter (d) of the RMF model with respect to the value using the base model. The figure is taken from Ref. [50].

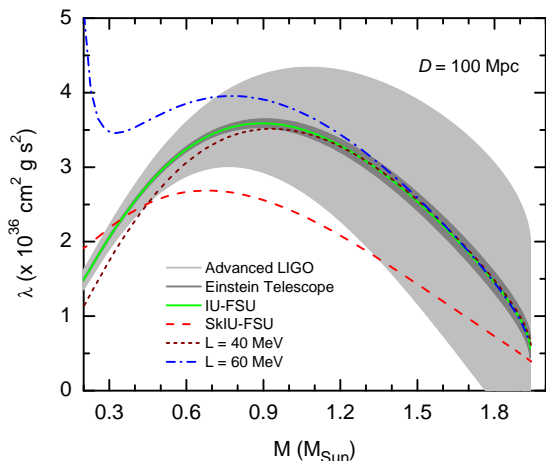


Fig. 5. (Color online) Tidal polarizability λ of a single neutron star as a function of neutron-star mass for a range of EOS that allow various stiffness of symmetry energies. A crude estimate of uncertainties in measuring λ for equal mass binaries at a distance of $D = 100$ Mpc is shown for the Advanced LIGO [83] (shaded light-grey area) and the Einstein Telescope [84] (shaded dark-grey area). This result was first reported in Ref. [50].

sufficient to assume that neutron stars consist of only neutrons (n), protons (p), electrons (e) and muons (μ) in β -equilibrium [50].

In Ref. [50], we examined sensitivity of the tidal polarizability λ of a $1.4M_\odot$ neutron star to the variations of SNM properties and the slope of the symmetry energy around ρ_0 as shown in Fig. 4 and Table 1. The changes of λ relative to the values for our base RMF model are

Table 1. Predictions for the properties of a 1.4 solar mass neutron star using the seventeen EOSs considered in this paper. The properties of nuclear matter around our base parametrization are systematically varied to obtain flexible range of the EOSs, but within the available theoretical, experimental and observational constraints. The first column reports the name of the EOS with a particular nuclear property and/or ζ -parameter indicated. The radii are in units of km, the tidal polarizability in $10^{36} \text{ cm}^2 \text{ g s}^2$.

EOS	R	k_2	λ	$\Delta\lambda/\lambda$
Base	12.88	0.0879	3.115	—
$K = 210$ MeV	12.82	0.0858	2.974	-4.52 %
$K = 220$ MeV	12.85	0.0869	3.046	-2.19 %
$K = 240$ MeV	12.91	0.0890	3.183	+2.21 %
$K = 250$ MeV	12.94	0.0900	3.258	+4.59 %
$M^* = 0.580 M$	12.71	0.1033	3.427	+10.01 %
$M^* = 0.595 M$	12.83	0.0943	3.271	+ 5.02 %
$M^* = 0.625 M$	12.89	0.0831	2.957	- 5.06 %
$M^* = 0.640 M$	12.88	0.0792	2.800	-10.12 %
$L = 42$ MeV	12.33	0.1677	3.089	-0.83 %
$L = 46$ MeV	12.64	0.1635	3.096	-0.58 %
$L = 54$ MeV	13.07	0.1582	3.140	+0.80 %
$L = 58$ MeV	13.22	0.1564	3.170	+1.79 %
$\zeta = 0.0200$	13.01	0.0885	3.302	+6.00 %
$\zeta = 0.0225$	12.94	0.0882	3.204	+2.85 %
$\zeta = 0.0275$	12.81	0.0876	3.025	-2.90 %
$\zeta = 0.0300$	12.75	0.0873	2.938	-5.67 %

Table 2. Predictions for the properties of a 1.4 solar mass neutron star using the IU-FSU EOS with difference density dependence of the symmetry energy. The slopes of the symmetry energy are in units of MeV, radii are in units of km, and the tidal polarizability in $10^{36} \text{ cm}^2 \text{ g s}^2$. The relative percentage error $\Delta\lambda/\lambda$ is calculated with respect to the original IU-FSU parametrization [61].

EOS	L	R	k_2	λ	$\Delta\lambda/\lambda$
IU-FSU	47.2	12.49	0.0930	2.828	—
IU-FSU-min	40.0	12.20	0.1054	2.841	+ 0.46 %
IU-FSU-max	60.0	13.07	0.0761	2.906	+ 2.76 %
SkIU-FSU	47.2	11.71	0.0753	1.657	-41.41 %

shown for the remaining RMF EOSs. It is very interesting to see that the tidal polarizability is rather insensitive to the variation of L within the constrained range, although it changes up to $\pm 10\%$ with K_0 , M^* and ζ within their individual uncertain ranges.

While the averaged mass is $M = 1.33 \pm 0.05 M_\odot$, neutron stars in binaries have a broad mass distribution [85]. It is thus necessary to investigate the mass dependence of the tidal polarizability. Whereas what can be measured for a neutron star binary of mass M_1 and M_2 is the mass-weighted tidal polarizability [76]

$$\tilde{\lambda} = \frac{1}{26} \left[\frac{M_1 + 12M_2}{M_1} \lambda_1 + \frac{M_2 + 12M_1}{M_2} \lambda_2 \right], \quad (14)$$

for the purpose of this study it is sufficient to consider binaries consisting of two neutron stars with equal masses. In Fig. 5 the tidal polarizability λ as a function of neutron-star mass for a range of EOSs is shown. Very interestingly, it is seen that the IU-FSU and SkIU-FSU models which are different only in their predictions for the nuclear symmetry energy above about $1.5\rho_0$ (see Fig. 1) lead to significantly different λ values in a broad mass range from 0.5 to $2 M_\odot$. More quantitatively, a 41% change in λ from 2.828×10^{36} (IU-FSU) to 1.657×10^{36} (SkIU-FSU) is observed for a canonical neutron star of $1.4 M_\odot$ (See Table 2). For a comparison, we notice that this effect is as strong as the symmetry energy effect on the late time neutrino flux from the cooling of proto-neutron stars [49]. However, we should note that the SNM components of the EOSs used in Ref. [49] are also significantly different and therefore a further systematic test may be desirable. Moreover, it is shown that the variation of L on 40 to 60 MeV as allowed by the PNM constraints has a very small effect on the tidal polarizability λ of massive neutron stars, which is consistent with the results shown in Fig. 4. On the other hand, the L parameter affects significantly the tidal polarizability of neutron stars with $M \leq 1.2M_\odot$. These observations can be easily understood. From Eq. (8) the Love number k_2 is essentially determined by the compactness parameter M/R and the function $y(R)$. Both of them are obtained by integrating the EOS all the way from the core to the surface. Since the saturation density approximately corresponds to the central density of a $0.3M_\odot$ neutron star, one thus should expect that only the Love number of low-mass neutron stars to be sensitive to the EOS around the saturation density. However, for canonical and more massive neutron stars, the central density is higher than 3 to 4 saturation density ρ_0 , and therefore both the compactness M/R and $y(R)$ show stronger sensitivity to the variation of EOS at supra-saturation densities. Since all the EOSs for SNM at supra-saturation densities have already been constrained by the terrestrial nuclear physics data and required to give a maximum mass about $2M_\odot$ for neutron stars, the strongest effect on calculating the tidal polarizability of massive neutron stars should therefore come from the high-density behavior of the symmetry energy.

It has been suggested that the Advanced LIGO-Virgo detector may potentially measure the tidal polarizability of binary neutron stars with a moderate accuracy. To test whether planned GW detectors are sensitive enough to measure the predicted effects of high-density symmetry energy on the tidal polarizability, as an example, we estimate uncertainties in measuring λ for equal mass binaries at an optimally-oriented distance of $D = 100$ Mpc [76, 86] using the same approach as detailed in Refs. [76, 82]. For example, for point-particle models of binary inspiral, Ref. [71] showed that one can obtain analytical gravitational waveform accurate to 2-3 post-Newtonian (PN) order. The tidal contribution to the GW signal is then found to be accurate to less than 10 %. Current uncertainties in

the determination of λ is estimated as [76]:

$$\Delta\tilde{\lambda} = \alpha \left(\frac{M}{M_\odot}\right)^{2.5} \left(\frac{M_2}{M_1}\right)^{0.1} \left(\frac{f_{\text{end}}}{\text{Hz}}\right)^{-2.2} \left(\frac{D}{100 \text{ Mpc}}\right), \quad (15)$$

where $M = M_1 + M_2$ is the total mass of the binary, $\alpha = 1.0 \times 10^{42} \text{ cm}^2 \text{ g s}^2$ for a single Advanced LIGO-Virgo detector, and $\alpha = 8.4 \times 10^{40} \text{ cm}^2 \text{ g s}^2$ for a single Einstein Telescope detector. These uncertainties are shown for the Advanced LIGO-Virgo (shaded light-grey area) and the Einstein Telescope (shaded dark-grey area) in Fig. 5 assuming the IU-FSU as the base model.

It is seen that discerning between high-density symmetry energy behaviors is at the limit of Advanced LIGO-Virgo's sensitivity for stars of mass $1.4M_\odot$ and below based on the currently estimated uncertainty, and it is possible that a rare but nearby binary system may be found and provide a much more tighter constraint [76]. While discoveries of binary neutron star systems PSR B1913+16 and PSR J0737-3039 at a nearby location (6.4 kpc and 0.6 kpc respectively) reminds us that such a possibility may not be likely, the rate estimates for detection of binary neutron stars are found to be very small for a single Advanced LIGO-Virgo interferometer [76]. Nonetheless, measurements for binaries consisting of light neutron stars can still help further constrain the symmetry energy around the saturation density. On the other hand, it is noteworthy that the narrow uncertain range for the proposed Einstein Telescope even at very large distances will enable it to stringently constrain the symmetry energy especially at high densities.

3.2 Gravitational waves from elliptically deformed pulsars

Rotating neutron stars are major candidates for sources of continuous gravitational waves in the frequency bandwidth of the current laser interferometric detectors [86]. According to general relativity any rotating axial-asymmetric objects should radiate gravitationally. There are several mechanisms that may lead to an axial asymmetry in neutron stars [87]:

- a) Anisotropic stress built up during the crystallization period of the solid neutron star crust may support static "mountains" on the surface of neutron stars [88];
- b) Due to its violent formation in supernova the rotational axis of a neutron star may not necessarily coincide with the principal axis of the moment of inertia, which results in a neutron star precession [89, 90];
- c) Since neutron stars possess strong magnetic fields they can create a magnetic pressure, which in turn may distort the star. This is possible only if the magnetic field axis is not aligned with the axis of rotation, which is always the case for pulsars [91].

These processes generally result in a triaxial neutron star configuration. Gravitational waves are then characterized by a tiny dimensionless strain amplitude, h_0 , which

depends on the degree to which the neutron star is deformed from axial symmetry [92]:

$$h_0 = \frac{16\pi^2 G}{c^4} \frac{\epsilon I_{zz} f^2}{r}, \quad (16)$$

where f is the rotation frequency of the neutron star, I_{zz} is its moment of inertia around the principal axis, $\epsilon = (I_{xx} - I_{yy})/I_{zz}$ is its equatorial ellipticity as defined in the literature on gravitational waves [86], and r is the distance from the source to the observer. The ellipticity is related to the neutron star maximum quadrupole moment through [93]

$$\epsilon = \sqrt{\frac{8\pi}{15}} \frac{Q_{22,\max}}{I_{zz}}. \quad (17)$$

Notice that the gravitational wave strain amplitude does not depend on the neutron star moment of inertia I_{zz} , and the total dependence upon the underlying EOS is entirely due to the maximum quadrupole moment, $Q_{22,\max}$. Using a chemically detailed model of the crust, Ref. [94] computes the maximum quadrupole moment for a neutron star

$$Q_{22,\max} = 2.4 \times 10^{38} \text{ g cm}^2 \left(\frac{\sigma_{\max}}{10^{-2}} \right) \left(\frac{R}{10 \text{ km}} \right)^{6.26} \left(\frac{1.4 M_{\odot}}{M} \right) \quad (18)$$

where σ_{\max} is the breaking strain of the crust. Although earlier studies have estimated the value of the breaking strain to be in the range of $\sigma_{\max} = [10^{-5} - 10^{-2}]$ [92], more recently using molecular dynamics simulations it was estimated that the breaking strain can be as large as $\sigma_{\max} \approx 0.1$, which is considerably larger than the previous findings [88]. Using a rather conservative value of $\sigma_{\max} = 0.01$, in a work involving one of us [87] we reported the first direct nuclear constraints on the gravitational wave signals to be expected from several pulsars. Particularly, it has been found that for several millisecond pulsars located at distances 0.18 kpc to 0.35 kpc from Earth, the maximal gravitational wave strain amplitude is in the range of $h_0 \sim [0.4 - 1.5] \times 10^{-24}$. The EOS used in Ref. [87] was calculated using the momentum dependent interaction (MDI). The high density component of the symmetry energy in MDI is controlled by a single parameter x that is introduced in the single-particle potential of the MDI EOS. In calculating boundaries of the possible neutron star configurations, only EOSs that are consistent with the isospin diffusion laboratory data and measurements of the neutron skin thickness in ^{208}Pb [95, 96] were used that suggest the x -parameter is in the range of $x = -1$ (stiff) and $x = 0$ (soft). It was then shown that EOSs with stiff symmetry energy, such as MDI with $x = -1$, results in less compact stellar models, and hence more deformed neutron stars. It is of course reasonable to expect that more compact stellar configurations as predicted by the models with softer symmetry energy would be more resistant to any kind of deformation [87]. Also, in a work involved two of us [97] we have demonstrated that pasta phases can play essential role on the maximum quadrupole ellipticity sustainable by the crust. In particular, for EOSs with density slope of the symmetry energy

of $L < 70$ MeV, depending on the pasta phases the effect on the maximum quadrupole ellipticity can be as large as an order of magnitude.

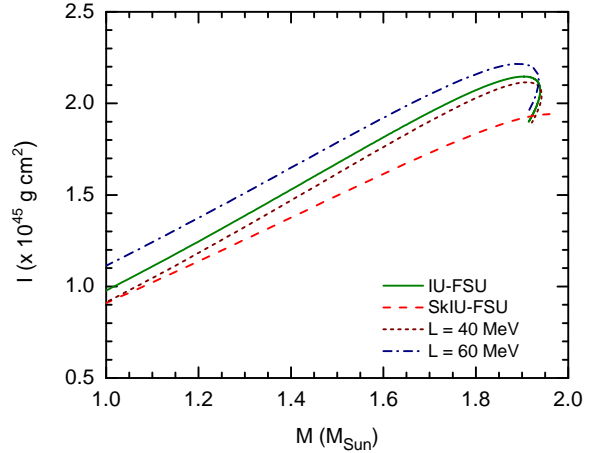


Fig. 6. (Color online) Neutron star moment of inertia as calculated using Eqn. (19) using various EOSs with different stiffness of symmetry energies.

In Fig. 6 we display the neutron star moment of inertia calculated using a simple empirical relationship proposed by Ref. [98]:

$$I \simeq 0.237MR^2 \left[1 + 4.2 \left(\frac{M \text{ km}}{M_{\odot} R} \right) + 90 \left(\frac{M \text{ km}}{M_{\odot} R} \right)^4 \right] \quad (19)$$

This expression is shown to hold for a wide class of equations of state that do not exhibit considerable softening and for neutron star models above $1 M_{\odot}$. In Fig. 7 we display the maximum quadrupole moment calculated via

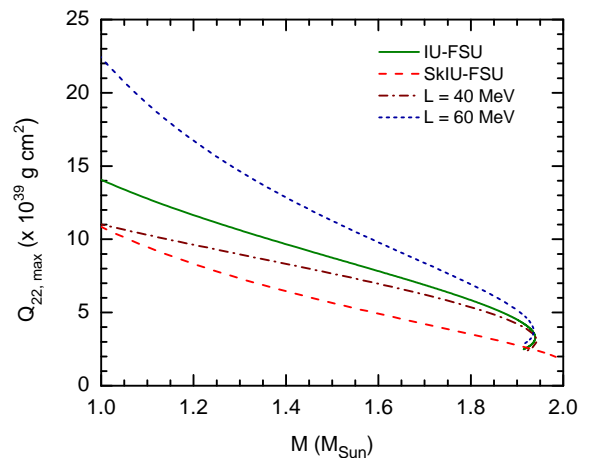


Fig. 7. (Color online) Neutron star maximum quadrupole moment as calculated using Eqn. (18).

Eqn. (18), where we chose the value of the breaking strain as $\sigma_{\max} = 0.1$. We notice that both moment of inertia and the maximum quadrupole moment are sensitive to the density dependence of the symmetry energy. Particularly, low-mass neutron stars exhibit a strong sensitivity to the density dependence of the nuclear symmetry energy around saturation density, while massive neutron stars are more sensitive to the high-density component of the symmetry energy. When the general relativistic expression for the moment of inertia is used the result remains the same qualitatively, although it slightly changes quantitatively. We emphasize that the gravitational strain amplitude as calculated above is independent of the moment of inertia, and strongly depends on the axial-asymmetric quadrupole moment. In Fig. 8 we show the maximum ellipticity that

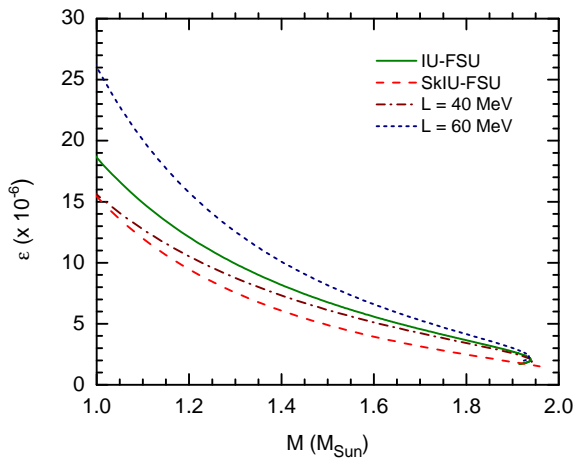


Fig. 8. (Color online) Ellipticity as a function of the neutron star mass.

can be supported by the crust as a function of the stellar mass. Since ϵ is proportional to the quadrupole moment scaled by the moment of inertia, it decreases with increasing stellar mass. It is seen that models with stiff symmetry energy favor the larger crust “mountains”. There is also a significant difference for the calculated deformations using models with the same symmetry energy at saturation, but different high-density component (IU-FSU and SkIU-FSU) of the symmetry energy.

Finally, in Table 3 we report calculated upper limits on gravitational wave strain amplitude for various pulsars and compare the results with observational upper limits. The results illustrate the relationships discussed above. It is shown that the gravitational wave strain amplitude is very sensitive to the density dependence of the symmetry energy. This sensitivity is most apparent in the Eqn. (18) of the maximum quadrupole moment that depends on the 6.26th power of the stellar radius. While gravitational waves for low-mass neutron stars are sensitive to the density slope of the nuclear symmetry energy, this sensitivity weakens as the neutron star becomes more massive. For massive neutron stars the effect of the high-density compo-

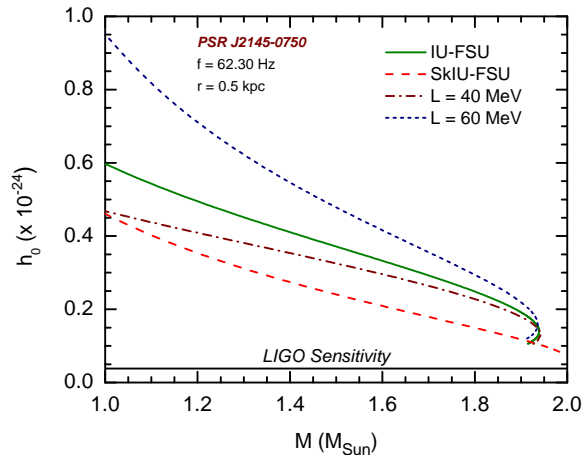


Fig. 9. (Color online) Gravitational wave strain amplitude as a function of the neutron star mass. The result is shown for pulsar J2145–0750.

nent of the symmetry energy is dominant (Also see Fig. 9). The results in Table 3 suggest that at present the gravitational radiation from these pulsars should be within the detection capabilities of LIGO [99]. However, no signal detection from any of these targets were reported. The fact that such a detection has not been made yet deserves a few comments. First and most importantly, recall that in computing the upper limits on h_0 we have used the maximum value for the breaking strain of the neutron star crust $\sigma = 0.1$ [88], which might be too optimistic. Even if the value is right, it is very important to understand that this does not suggest that neutron stars will have deformations of such magnitude. In fact, the main problem is to provide a reasonable scenario that leads to the development of large deformations [100]. In this regard, accretion-powered pulsars could be promising sources due to the expected asymmetry of the accretion flow near the stellar surface. However the required modeling for accreting systems have not been easy because of their complicated dynamics. Besides, none of the pulsars presented in Table 3 are known to be in accreting systems [101]. Second, we have assumed a fixed $1.4M_{\odot}$ neutron star, while h_0 depends on the neutron star mass and gets much smaller for massive neutron stars (See Fig. 9). Last, distance estimates that are based on dispersion measure could also be wrong by a factor 2 – 3 [86]. Obviously, much work remains to be done in the observational front, in order to extract information on the density dependence of the nuclear symmetry energy.

3.3 Neutron star oscillations

In a similar way that helioseismology studies the internal structure and dynamics of our Sun, neutron star seismology can be used to obtain information on various properties of neutron stars, and therefore to extract the EOS of neutron-rich matter [102]. Depending on their characteristics, neutron-star oscillation modes are usually divided

Table 3. Properties of the nearby pulsars considered in this study. The first column identifies the pulsar. The remaining columns are rotational frequency, distance to Earth, the observed [99] and the calculated upper limits on the gravitational wave strain amplitude. Notice that the masses of most of these pulsars are presently unknown and therefore we have adopted a canonical $1.4M_{\odot}$ mass neutron star in calculating the gravitational wave strain amplitudes, which are all given in units of 1.0×10^{-24} .

Pulsar	f (Hz)	r (kpc)	h_0^{ob}	h_0^{th} (IU-FSU)	h_0^{th} (IU-FSU-min)	h_0^{th} (IU-FSU-max)	h_0^{th} (SkIU-FSU)
J0437–4715	173.69	0.1	0.5730	15.9590	13.7350	21.2256	10.6567
J0613–0200	326.60	0.5	0.1110	11.2855	9.7127	15.0097	7.5359
J0751+1807	287.46	0.6	0.1640	7.2855	6.2702	9.6898	4.8649
J1012+5307	190.27	0.5	0.0694	3.8303	3.2965	5.0943	2.5577
J1022+1001	60.78	0.4	0.0444	0.4886	0.4205	0.6498	0.3262
J1024–0719	193.72	0.5	0.0501	3.9704	3.4171	5.2807	2.6513
J1455–3330	125.20	0.7	0.0515	1.1846	1.0195	1.5755	0.7910
J1730–2304	123.11	0.5	0.0593	1.6035	1.3801	2.1327	1.0708
J1744–1134	245.43	0.5	0.1100	6.3730	5.4848	8.4761	4.2556
J1857+0943	186.49	0.9	0.0727	2.0442	1.7593	2.7188	1.3650
J2019+2425	254.16	0.9	0.0923	3.7969	3.2678	5.0499	2.5354
J2124–3358	202.79	0.2	0.0485	10.8773	9.3614	14.4668	7.2634
J2145–0750	62.30	0.5	0.0383	0.4106	0.3534	0.5462	0.2742
J2322+2057	207.97	0.8	0.1120	2.8600	2.4614	3.8038	1.9098

into toroidal and spherical modes. Further, based on the nature of the restoring force these modes are classified as follows:

- 1) *f* fundamental modes, or *f*-modes, associated with the global oscillation of the fluid, whose frequencies are in the range of 1-10 kHz;
- 2) *g* gravity modes, or *g*-modes associated with the fluid buoyancy, whose frequencies are in the range of 2-100 Hz;
- 3) *p* pressure modes, or *p*-modes, associated with pressure gradient and whose frequencies lie in the range of few kHz;
- 4) *r* rotational modes (also known as *Rossby* modes), or *r*-modes, associated with the Coriolis force which acts as a restoring force along the surface, and whose frequency depends on the stars rotational frequency;
- 5) purely general-relativistic gravitational wave modes, or *w*-modes, associated with the curvature of space-time and typically have a very high frequency of above 7 kHz.

There has recently been considerable interest and effort in extracting information on the density dependence of the symmetry energy from analyzing various neutron star observations associated with oscillation modes. In particular, it was shown in Ref. [97, 103, 104, 105] that by identifying quasiperiodic oscillation (QPO) following giant magnetar flares in soft gamma repeaters with the torsional oscillations of the crust it may be possible to extract the density dependence of the symmetry energy (Also see the contributions to this volume by Iida & Oyamatsu). For example, Ref. [103] have calculated the frequency of shear oscillations of the neutron star crust, and showed that they depend sensitively on the slope of the symmetry energy at saturation. By using a consistent treatment of the EOS of crust and core, but an approximate method for the description of the torsional modes in a work involved two of us [97] we showed that one can associate the observed

QPO frequencies with the fundamental shear mode, if the density slope of the symmetry energy is $L < 65$ MeV. Soon after, using a more sophisticated calculation for the crustal frequencies, but an inconsistent EOS of the crust and core, Ref. [104] arrived at a conclusion that the value of density slope should lie in the range of $100 < L < 130$ MeV. In their later analysis Ref. [105] also reported a more conservative range of $L \geq 47.4$ MeV, depending on the identification of the fundamental crust modes. These results suggest that such oscillations could be a powerful probe of the symmetry energy at saturation density, but that it is important to incorporate a sophisticated model of the crust, consistent calculations of the EOS of crust and core and the effects of the high magnetic fields into the analysis.

Due to their purely general-relativistic nature, *w*-modes have also become the focal point of many investigations [106, 107]. In particular, it was shown that the density dependence of the nuclear symmetry energy has a clear imprint on both the frequency and the damping time of the axial *w*-modes [106]. Although the *w*-mode frequencies are outside the bandwidth of the current gravitational wave detectors, major upgrades will be completed over the coming years that will significantly improve sensitivity required to detect gravitational waves over a much broader band [83, 84].

In this contribution we will concentrate on the *r*-mode of the oscillation, whose study has increased significant attention soon after their first relativistic calculations [108, 109].

3.3.1 The *r*-mode instability in neutron stars

Theoretically, rotating neutron stars cannot have a spin frequency larger than their Kepler frequency, Ω_K . This is an absolute upper limit on the stars rotation rate above which the matter gets ejected from the star's equator.

However, the available observational data suggests that the spin-up of neutron stars from accretion is limited to frequencies much lower $\Omega/\Omega_K < 0.1$. One possible explanation is the Chandrasekhar-Friedmann-Schutz (CFS) instability of the r -mode oscillations. This instability might play an important role in generating gravitational waves from the accretion-powered millisecond pulsars in low-mass X-ray binaries (LMXBs). The CFS instability sets an upper limit on the rotation frequency, above which r -modes are unstable to gravitational radiation. The r -mode instability window depends on the competition between the gravitational radiation and the viscous dissipation timescales, where gravitational radiation makes the r -mode amplitude grow and viscosity in the fluid damps the amplitude, stabilizing the mode. It was first shown in Refs. [110,108] that for all slowly rotating neutron stars, gravitational radiation timescales exceed the one due to viscous damping. In what follows we will use the same approach as discussed in Ref. [111,112,113,114]. By assuming that the crust of the neutrons star is perfectly rigid, one can find an upper limit on the instability window. This is because the viscous boundary layer between the fluid core and the rigid crust is maximally dissipative. In the realistic case of more elastic crust, the dissipation from the core-crust boundary decreases and therefore widens the instability window. In a recent work involving some of us [111], we studied the sensitivity of the r -mode instability to the density dependence of the symmetry energy. In particular, by employing a simple model of a neutron star with a perfectly rigid crust constructed with a set of crust and core EOS that span the range of nuclear experimental uncertainty in the symmetry energy, we found that EOSs characterized by the density slope L of smaller than 65 MeV are more consistent with the observed frequencies in LMXBs. In this work the electron-electron scattering was considered as the main dissipative mechanism. However, considering a different approach in which the viscous dissipation was assumed to operate throughout the whole core of the star instead of at the crust-core boundary layer, and using both microscopic and phenomenological approaches to the nuclear EOS, Ref. [115] concluded that observational data seem to favor values of density slope larger than 50 MeV. We should make the caveat that both studies use greatly simplified models of the instability, and rely on an interpretation of observations that is only one of several possible.

According to Ref. [110] the gravitational radiation timescale can be evaluated using the following expression:

$$\frac{1}{\tau_{\text{GR}}} = \frac{32\pi G \Omega^{2l+2}}{c^{2l+5}} \frac{(l-1)^{2l}}{[(2l+1)!!]^2} \left(\frac{l+2}{l+1}\right)^{2l+2} \times \int_0^{R_t} \mathcal{E} r^{2l+2} dr, \quad (20)$$

where Ω is the stellar angular frequency and $\mathcal{E} \equiv \mathcal{E}(r)$ is the energy density profile of the star. The viscous damping timescale due to viscous dissipation at the core-crust boundary layer assuming a perfectly rigid crust and fluid

core can be calculated using [114]

$$\tau_v = \frac{2^{l+1}(l+1)!}{l(2l+1)!! \mathcal{I}_l c R_t^{2l+2} \sqrt{\mathcal{E}_t \Omega \eta_t}} \int_0^{R_t} \mathcal{E} r^{2l+2} dr. \quad (21)$$

where the integral

$$\mathcal{I}_l = \int_0^\pi \sin^{2l-1} \theta (1 + \cos \theta)^2 \sqrt{|\cos \theta - 1/(l+1)|} d\theta, \quad (22)$$

and the subscript ‘‘t’’ is used to identify quantities at the core-crust interface. Here we only consider quadrupole modes of $l = 2$, for which $\mathcal{I}_2 \approx 0.80411$. For hot neutron stars with temperature above $T = 10^9$ K, it is expected that the neutron-neutron scattering becomes the dominant dissipation mechanism, and its viscosity is expressed by

$$\eta_{nn} = k_{nn} \rho^{9/4} T^{-2}, \quad (23)$$

where

$$k_{nn} = 347 \text{ g}^{-5/4} \text{ cm}^{23/4} \text{ K}^2 \text{ s}^{-1}, \quad (24)$$

and ρ is the mass density. As the temperature drops below about 10^9 K, the neutron star shear viscosity is then dominated by the electron-electron scattering, which also depends on density and temperature:

$$\eta_{ee} = k_{ee} \rho^2 T^{-2}, \quad (25)$$

where

$$k_{ee} = 6.0 \times 10^6 \text{ g}^{-1} \text{ cm}^5 \text{ K}^2 \text{ s}^{-1}, \quad (26)$$

The critical rotation frequency Ω_c is then defined when $\tau_{\text{GR}} = \tau_v$. In this work we do not consider new-born stars, whose temperatures are usually above $T > 10^9$ K and for which the bulk viscosity would be the dominant dissipation mechanism.

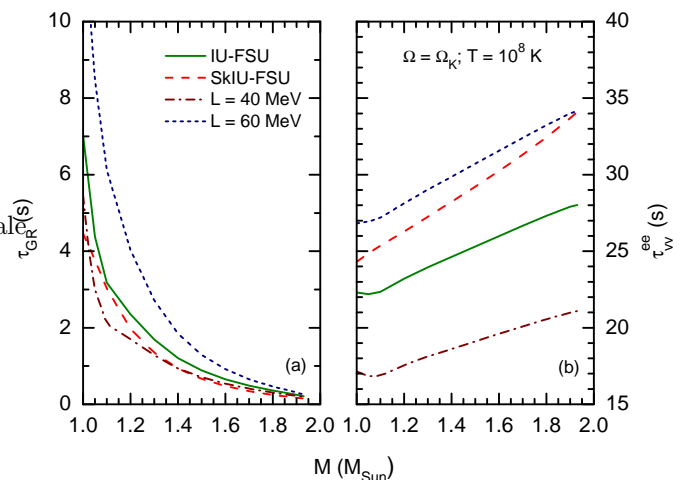


Fig. 10. (Color online) Timescales for the (a) gravitational radiation driven r -mode instability and (b) corresponding viscous dissipation due to the electron-electron scattering at the core-crust interface as a function of stellar mass.

In Fig. 10 the timescales for the gravitational radiation (left window) and the shear viscosity (right window), which dissipates the r -mode instability are shown as a function of stellar mass. The stellar structure is modeled with a rigid crust [111] for the adopted EOSs, and the shear viscosity of the boundary layer is taken to be dominated by electron-electron scattering. Both timescales depend on the stellar mass with gravitational timescale being a decreasing function of the neutron star mass, whereas the viscous damping timescale is an increasing function of the stellar mass. Although both the gravitational radiation timescale and the viscous damping timescale seems to be more sensitive to the density dependence of the symmetry energy at saturation, an apparent sensitivity emerges for the high-density component of the symmetry energy in the viscous damping timescale only. Indeed, we should note that these timescales strongly depend on the core-to-crust transition properties, which occurs at about half saturation density. The sensitivity to the high density component of the symmetry energy only enters through the integrals shown in Eqns. (20)-(21) which are evaluated numerically.

process for normal nucleons (left stars) or by the modified Urca process for neutrons being superfluid and protons being superconducting (right stars) in the core [116]. It is shown that for a canonical neutron star, all considered LMXBs lie outside the instability window and is consistent with the observation that no r -mode is currently excited in LMXBs, due to the shortness in duration of the unstable r -mode activity [117,118]. However, for the massive neutron stars, some of the stars fall within the instability region constrained by the EOSs. Considering that LMXBs should fall below the instability window and assuming that current observational interpretation is correct, then within our simple model one can conclude from Fig. 11 that one of the following must hold: (a) stars in LMXBs are not so massive; and either (b) the high-density component of the symmetry energy is soft, or (c) the density slope of the symmetry energy at saturation is $L < 60$ MeV. Suppose that the short recurrence time LMXBs (sLMXBs) presented in the Fig. 11 are identified to be massive, and the density slope of the symmetry energy L constrained by terrestrial experiments is equal or larger than 60 MeV, then one would conclude that the symmetry energy must be soft at higher densities.

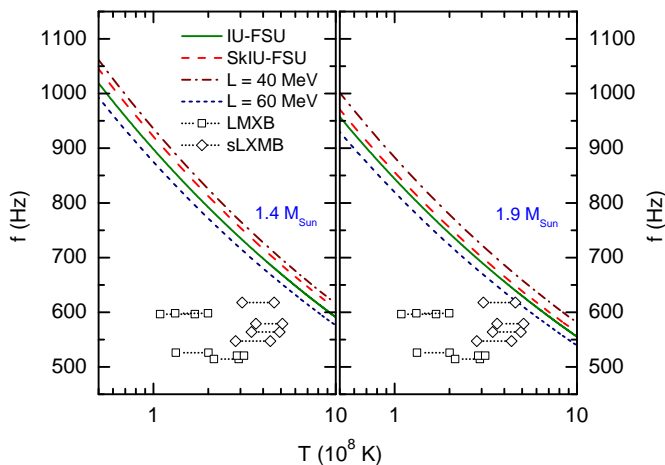


Fig. 11. (Color online) The r -mode instability window for a 1.4-solar mass (left window) and a 1.9-solar mass neutron stars are shown for various EOSs discussed in the text. Also the location of the observed low mass X-ray binaries (LMXBs) and short recurrence time LMXBs (sLMXB) are shown [116].

Since the masses of the neutron stars in low-mass X-ray binaries (LMXBs) are not measured as accurately as those in certain binary NS-NS or NS-White Dwarf (WD) systems, we explore the position of LMXBs in the r -mode instability window, defined as the region in frequency-temperature space above the critical frequency, in both canonical and massive neutron stars. The r -mode instability window for neutron stars of $1.4M_{\text{Sun}}$ and $1.9M_{\text{Sun}}$ are displayed in the left and right windows of Fig. 11, respectively. The core temperatures T of the LMXBs are derived from their observed accretion luminosity assuming the cooling is either dominated by the modified Urca

4 Conclusions

In this survey we have examined the sensitivity of various neutron star-sourced gravitational wave signals to the density dependence of symmetry energy, with a special emphasis on the high density behavior of the symmetry energy. Specifically, we have addressed the sensitivity of gravitational wave signals from tidally polarized neutron stars, accretion-induced neutron star ellipticities, and r -mode oscillations to the EOSs of neutron-rich matter.

To study this sensitivity we have used various EOSs for neutron-rich nucleonic matter satisfying the latest constraints from terrestrial nuclear experiments, state of the art nuclear many-body calculations for EOS of PNM, and astrophysical observation. We have used this same set of EOSs to test each of the different GW sources, so that their relative sensitivities to dense nuclear matter properties may be consistently compared.

We have found that among various gravitational wave signatures the tidal polarizability of neutron stars in coalescing binaries is particularly sensitive to the high-density behavior of the nuclear symmetry energy. Moreover, tidal polarizability is relatively insensitive to variations of the EOS of SNM and the density dependence of the symmetry energy around saturation density within their remaining experimental and model uncertainty ranges.

Next, we calculated the gravitational wave strain amplitude from neutron stars elliptically deformed by crustal mountains. The exact calculation of the neutron star quadrupole moment (and therefore the gravitational wave strain amplitude) requires a detailed knowledge of the neutron star crust. Within a simple approximation, our estimations show that it may be possible to disentangle the effect of the high-density component of the symmetry energy from its density dependence around saturation density for

the very massive neutron stars only. Much works need to be done to completely understand the physics of neutron star crust, in particular its ability to support large ellipticities, but it is clear that observations of gravitational waves from accreting neutron stars is a promising avenue towards constraining the EOS of neutron-rich nucleonic matter.

Lastly, we have explored the dependence of the r -mode instability window on the high-density component of the symmetry energy. We have analyzed and confirmed the previous findings that the instability window is mostly sensitive to the EOS at around the crust-core transition density, and therefore to the density dependence of the symmetry energy around saturation density. The knowledge of high density behavior of the symmetry energy becomes very important, especially when one combines future stringent experimental constraints on the value of L with existing and future observations of LMXBs. Within this simple model, we have found that EOSs characterized by L value smaller than 60 MeV are consistent with the observations. In particular, if large values of L are favored from forthcoming terrestrial experiments, then models with stiff symmetry energy at high densities would be ruled out.

Future measurements of the gravitational wave signals will therefore be utterly important in constraining stringently the high-density behavior of nuclear symmetry energy, and thus the nature of dense neutron-rich nucleonic matter.

Acknowledgments

This work was supported in part by the National Aeronautics and Space Administration under Grant No. NNX11AC41G issued through the Science Mission Directorate, and the National Science Foundation under Grant No. PHY-1068022.

References

1. The 2007 US NSAC Long Range Plan, <http://science.energy.gov/np/nsac/>.
2. P. B. Demorest, T. Pennucci, S. M. Ransom, M. S. E. Roberts, and J. W. T. Hessels, *Nature* **467**, (2010) 1081.
3. J. Antoniadis, P. C. Freire, N. Wex, T. M. Tauris, R. S. Lynch, *et al.*, *Science* **340**, (2013) 6131.
4. P. Danielewicz, R. Lacey, and W. G. Lynch, *Science* **208**, (2002) 1592.
5. J. M. Lattimer, and M. Prakash, *Phys. Rept.* **333** (2000), 121.
6. J. M. Lattimer, and M. Prakash, *Science* **304** (2004), 536.
7. J. M. Lattimer and Y. Lim (2012), *Astrophys. J.* **771** (2013), 51.
8. C. Xu, B.-A. Li, and L.-W. Chen, *Phys. Rev. C* **82** (2010), 054607.
9. W. G. Newton, M. Gearheart, and B.-A. Li (2011), *Astrophys. J. Suppl.* **204** (2013), 9.
10. A. W. Steiner and S. Gandolfi, *Phys. Rev. Lett.* **108** (2012), 081102.
11. M. Dutra, O. Lourenço, J. S. Sà Martins, A. Delfino, J. R. Stone, and P. D. Stevenson, *Phys. Rev. C* **85** (2012), 035201.
12. M. Tsang *et al.*, *Phys. Rev. C* **86** (2012), 015803.
13. F. J. Fattoyev, W. G. Newton, J. Xu, and B.-A. Li, *Phys. Rev. C* **86** (2012), 025804.
14. F. J. Fattoyev, and J. Piekarewicz, arXiv:1306.6034 (2013).
15. M. Kutschera, *Phys. Lett. B* **340** (1994), 1.
16. S. Kubis and M. Kutschera, *Acta Phys. Polon. B* **30** (1999), 2747.
17. S. Kubis and M. Kutschera, *Nucl. Phys. A* **720** (2003), 189.
18. D.-H. Wen, B.-A. Li, and L.-W. Chen, *Phys. Rev. Lett.* **103** (2009), 211102.
19. H. K. Lee, B.-Y. Park, and M. Rho, *Phys. Rev. C* **83** (2011), 025206.
20. B.-A. Li, L.-W. Chen, and C. M. Ko, *Phys. Rept.* **464** (2008), 113.
21. B. A. Brown, *Phys. Rev. Lett.* **85** (2000), 5296.
22. A. Szmaglini, W. Wojcik, and M. Kutschera, *Acta Phys. Polon. B* **37** (2006), 277.
23. A. E. L. Dieperink, Y. Dewulf, D. Van Neck, M. Waroquier, and V. Rodin, *Phys. Rev. C* **68** (2003), 064307.
24. A. W. Steiner, M. Prakash, J. M. Lattimer, and P. J. Ellis, *Phys. Rept.* **411** (2005), 325.
25. C.-H. Lee, T. T. S. Kuo, G. Q. Li, and G. E. Brown, *Phys. Rev. C* **57** (1998), 3488.
26. C. J. Horowitz and J. Piekarewicz, *Phys. Rev. Lett.* **86** (2001), 5647.
27. L.-W. Chen, C. M. Ko, and B.-A. Li, *Phys. Rev. C* **76** (2007), 054316.
28. Z. H. Li, U. Lombardo, H.-J. Schulze, W. Zuo, L. W. Chen, and H. R. Ma, *Phys. Rev. C* **74** (2006), 047304.
29. V. R. Pandharipande and V. K. Garde, *Phys. Lett. B* **39** (1972), 608.
30. B. Friedman and V. R. Pandharipande, *Nucl. Phys. A* **361** (1981), 502.
31. R. B. Wiringa, V. Fiks, and A. Fabrocini, *Phys. Rev. C* **38** (1988), 1010.
32. N. Kaiser, S. Fritsch, and W. Weise, *Nucl. Phys. A* **697** (2002), 255.
33. P. G. Krastev and F. Sammarruca, *Phys. Rev. C* **74**, (2006) 025808.
34. E. Chabanat, J. Meyer, P. Bonche, R. Schaefer, and P. Haensel, *Nucl. Phys. A* **627** (1997), 710.
35. J. R. Stone, J. C. Miller, R. Konciewicz, P. D. Stevenson, and M. R. Strayer, *Phys. Rev. C* **68** (2003), 034324.
36. L.-W. Chen, C. M. Ko, and B.-A. Li, *Phys. Rev. C* **72** (2005), 064309.
37. J. Decharge and D. Gogny, *Phys. Rev. C* **21** (1980), 1568.
38. C. B. Das, S. D. Gupta, C. Gale, and B.-A. Li, *Phys. Rev. C* **67** (2003), 034611.
39. D. T. Khoa, W. von Oertzen, and A. A. Ogloblin, *Nucl. Phys. A* **602** (1996), 98.
40. D. N. Basu, P. R. Chowdhury, and C. Samanta, *Nucl. Phys. A* **811** (2008), 140.
41. W. D. Myers and W. J. Swiatecki, *Acta Phys. Polon. B* **26** (1995), 111.
42. S. Banik and D. Bandyopadhyay, *J. Phys. G* **26** (2000), 1495.
43. P. R. Chowdhury, D. N. Basu, and C. Samanta, *Phys. Rev. C* **80** (2009), 011305.
44. C. Xu and B.-A. Li, *Phys. Rev. C* **81** (2010), 064612.

45. C. Xu, A. Li, and B.-A. Li, *J. Phys. Conf. Ser.* **420** (2013), 012090
46. Z. Xiao, B.-A. Li, L.-W. Chen, G.-C. Yong, and M. Zhang, *Phys. Rev. Lett.* **102** (2009), 062502.
47. P. Russotto *et al.*, *Phys. Lett. B* **697** (2011), 471.
48. W. Trautmann and H. H. Wolter, *Int. J. Mod. Phys. E* **21** (2012), 1230003.
49. L. F. Roberts, G. Shen, V. Cirigliano, J. A. Pons, S. Reddy, and S. E. Woosley, *Phys. Rev. Lett.* **108** (2012), 061103.
50. F. J. Fattoyev, J. Carvajal, W. G. Newton, and B.-A. Li, *Phys. Rev. C* **87**, (2013) 015806.
51. R. A. Hulse, and J. H. Taylor, *Astrophys. J.* **195** (1975), L51.
52. A. Schwenk and C. J. Pethick, *Phys. Rev. Lett.* **95** (2005), 160401.
53. E. van Dalen and H. Muther, *Phys. Rev. C* **80** (2009), 037303.
54. K. Hebeler and A. Schwenk, *Phys. Rev. C* **82** (2010), 014314.
55. S. Gandolfi, A. Y. Illarionov, S. Fantoni, F. Pederiva, and K. E. Schmidt, *Phys. Rev. Lett.* **101** (2008), 132501.
56. A. Gezerlis and J. Carlson, *Phys. Rev. C* **81** (2010), 025803.
57. E. N. I. Vidaña, A. Polls, and A. Ramos, *Phys. Rev. C* **65** (2002), 035804.
58. D. H. Youngblood, H. L. Clark, and Y.-W. Lui, *Phys. Rev. Lett.* **82** (1999), 691.
59. Y.-W. Lui, D. Youngblood, S. Shlomo, X. Chen, Y. Tokimoto *et al.*, *Phys. Rev. C* **83** (2011), 044327.
60. R. Furnstahl, J. J. Rusnak, and B. D. Serot, *Nucl. Phys. A* **632** (1998), 607.
61. F. J. Fattoyev, C. J. Horowitz, J. Piekarewicz, and G. Shen, *Phys. Rev. C* **82** (2010), 055803.
62. H. Mueller and B. D. Serot, *Nucl. Phys. A* **606** (1996), 508.
63. B. G. Todd-Rutel and J. Piekarewicz, *Phys. Rev. Lett.* **95** (2005), 122501.
64. S. Guillot, M. Servillat, N.A. Webb and R. E. Rutledge, *Astrophys. J.* **772** (2013), 7.
65. J. M. Lattimer, and A. W. Steiner, arXiv:1305.3242 (2013).
66. A. W. Steiner, J. M. Lattimer, and E. F. Brown, *Astrophys. J.* **722** (2010), 33.
67. F. Özel, G. Baym, and T. Guver, *Phys. Rev. D* **82** (2010), 101301.
68. V. Suleimanov, J. Poutanen, M. Revnivtsev, and K. Werner, *Astrophys. J.* **742** (2011), 122.
69. M. Burgay *et al.*, *Nature* **426** (2003), 531.
70. A. G. Lyne *et al.*, *Science* **303** (2004), 1153.
71. É. É. Flanagan and T. Hinderer, *Phys. Rev. D* **77** (2008), 021502.
72. T. Hinderer, *Astrophys. J.* **677** (2008), 1216.
73. T. Binnington and E. Poisson, *Phys. Rev. D* **80** (2009), 084018.
74. T. Damour and A. Nagar, *Phys. Rev. D* **80** (2009), 084035.
75. T. Damour and A. Nagar, *Phys. Rev. D* **81** (2010), 084016.
76. T. Hinderer, B. D. Lackey, R. N. Lang, and J. S. Read, *Phys. Rev. D* **81** (2010), 123016.
77. S. Postnikov, M. Prakash, and J. M. Lattimer, *Phys. Rev. D* **82** (2010), 024016.
78. L. Baiotti, T. Damour, B. Giacomazzo, A. Nagar, and L. Rezzolla, *Phys. Rev. Lett.* **105** (2010), 261101.
79. L. Baiotti, T. Damour, B. Giacomazzo, A. Nagar, and L. Rezzolla, *Phys. Rev. D* **84** (2011), 024017.
80. B. D. Lackey, K. Kyutoku, M. Shibata, P. R. Brady, and J. L. Friedman, *Phys. Rev. D* **85** (2012), 044061.
81. F. Pannarale, L. Rezzolla, F. Ohme, and J. S. Read, *Phys. Rev. D* **84** (2011), 104017.
82. T. Damour, A. Nagar, and L. Villain, *Phys. Rev. D* **85** (2012), 123007.
83. The Advanced LIGO gravitational wave detector, <https://www.advancedligo.mit.edu/>.
84. The Einstein Telescope project, <http://www.et-gw.eu/>.
85. F. Özel, D. Psaltis, R. Narayan, and A. S. Villarreal, *Astrophys. J.* **757** (2012), 55.
86. J. Abadie *et al.*, (LIGO Scientific Collaboration, Virgo Collaboration), *Class. Quant. Grav.* **27** (2010), 173001.
87. P. G. Krastev, B.-A. Li, and A. Worley, *Phys. Lett. B* **668** (2008), 1.
88. C. J. Horowitz, and K. Kadau, *Phys. Rev. Lett.* **102** (2009), 191102.
89. M. Zimmermann, and E. Szedenis, *Phys. Rev. D* **20** (1979), 351.
90. M. Zimmermann, *Phys. Rev. D* **21** (1980), 891.
91. S. Bonazzola, and E. Gourgoulhon, *Astron. Astrophys.* **312** (1996), 675.
92. B. Haskell, N. Andersson, D. I. Jones, and L. Samuelsson, *Phys. Rev. Lett.* **99** (2007), 231101.
93. B. J. Owen, *Phys. Rev. Lett.* **95** (2005), 211101.
94. G. Ushomirsky, C. Cutler, and L. Bildsten, *Mon. Not. R. Astron. Soc.* **319** (2000), 902.
95. B.-A. Li, and L.-W. Chen, *Phys. Rev. C* **72** (2005), 064611.
96. B.-A. Li, A. W. Steiner, *Phys. Lett. B* **642** (2006), 436.
97. M. Gearheart, W. G. Newton, J. Hooker, and B.-A. Li, *Mon. Not. R. Astron. Soc.* **418** (2011), 2343.
98. J. M. Lattimer, and B. F. Schutz, *Astrophys. J.* **629** (2005), 979.
99. B. P. Abbott *et al.*, (LIGO Scientific Collaboration, Virgo Collaboration), *Astrophys. J.* **713** (2010), 671.
100. N. Andersson *et al.*, *Gen. Relativ. Gravit.* **43** (2011), 409.
101. ATNF Pulsar Catalogue, <http://www.atnf.csiro.au/research/pulsar/psrcat/>
102. N. Andersson, and K. D., Kokkotas, *Phys. Rev. Lett.*, **677** (1996), 4134.
103. A. W. Steiner, and A. L. Watts, *Phys. Rev. Lett.* **103** (2009), 181101.
104. H. Sotani, K. Nakazato, K. Iida, and K. Oyamatsu, *Mon. Not. R. Astron. Soc.* **428** (2013), L21.
105. H. Sotani, K. Nakazato, K. Iida, and K. Oyamatsu, *Mon. Not. R. Astron. Soc.* **434** (2013), 2060.
106. D.-H. Wen, B.-A. Li, and P. G. Krastev, *Phys. Rev. C* **80** (2009), 025801.
107. W. Lin, B.-A. Li, J. Xu, C. M. Ko, D.-H. Wen, *Phys. Rev. C* **83** (2011), 045802.
108. N. Andersson, *Astrophys. J.*, **502** (1998), 708.
109. J. L. Friedman, and S. M. Morsink, *Astrophys. J.*, **502** (1998), 714.
110. L. Lindblom, B. J. Owen, and S. M. Morsink, *Phys. Rev. Lett.*, **80** (1998), 4843.
111. D.-H. Wen, W. G. Newton, and B.-A. Li, *Phys. Rev. C* **85** (2012), 025801.
112. L. Bildsten, and G. Ushomirsky, *Astrophys. J.* **529** (2000), L33.
113. N. Andersson, D. I. Jones, K. D. Kokkotas, and N. Stergioulas, *Astrophys. J.* **534** (2000), L75.
114. L. Lindblom, B. J. Owen, and G. Ushomirsky, *Phys. Rev. D* **62** (2000), 084030.

- 115. I. Vidaña, *Phys. Rev. C* **85** (2012), 045808.
- 116. W. C. G. Ho, N. Andersson, and B. Haskell, *Phys. Rev. Lett.*, **107** (2011), 101101.
- 117. Y. Levin, *Astrophys. J.*, **517** (1999), 328.
- 118. R. Bondarescu, S. A. Teukolsky, and I. Wasserman, *Phys. Rev. D* **76** (2007), 064019.